Earth Surface Processes and Landforms
Earth Surf. Process. Landforms **25**, 519–534 (2000)

RUNOFF GENERATION AND SEDIMENT PRODUCTION ON UNPAVED ROADS, FOOTPATHS AND AGRICULTURAL LAND SURFACES IN NORTHERN THAILAND

ALAN D. ZIEGLER*, ROSS A. SUTHERLAND, AND THOMAS W. GIAMBELLUCA
Geography Department, University of Hawaii, 2424 Maile Way, Honolulu, HI 96822, USA

Received 4 January 1999; Revised 20 September 1999; Accepted 21 October 1999

ABSTRACT

Rainfall simulation was used to examine runoff generation and sediment transport on roads, paths and three types of agricultural fields in Pang Khum Experimental Watershed (PKEW), in mountainous northern Thailand. Because interception of subsurface flow by the road prism is rare in PKEW, work focused on Horton overland flow (HOF). Under dry antecedent soil moisture conditions, roads generated HOF in *c*. 1 min and have event runoff coefficients (ROCs) of 80 per cent, during 45 min, *c*. 105 mm h^{-1} simulations. Runoff generation on agricultural fields required greater rainfall depths to initiate HOF; these surfaces had total ROCs ranging from 0 to 20 per cent. Footpaths are capable of generating erosion-producing overland flow within agricultural surfaces where HOF generation is otherwise rare. Paths had saturated hydraulic conductivity (K_s) values 80–120 mm h^{-1} lower than those of adjacent agricultural surfaces. Sediment production on roads exceeded that of footpaths and agricultural lands by more than eight times (1·23 versus $< 0{\cdot}15$ g J^{-1}). Typically, high road runoff volumes (owing to low K_s, *c*. 15 mm h^{-1}) transported relatively high sediment loads. Initial road sediment concentrations exceeded 100 g l^{-1}, but decayed with time as loose surface material was removed. Compared with the loose surface layer, the compacted, underlying road surface was resistant to detachment forces. Sediment concentration values for the road simulations were slightly higher than data obtained from a 165 m road section during a comparable natural event. Initial simulation concentration values were substantially higher, but were nearly equivalent to those of the natural event after 20 min simulation time. Higher sediment concentration in the simulations was related to differences in the availability of loose surface material, which was more abundant during the dry-season simulations than during the rainy season natural event. Sediment production on PKEW roads is sensitive to surface preparation processes affecting the supply of surface sediment, including vehicle detachment, maintenance activities, and mass wasting. The simulation data represent a foundation from which to begin parameterizing a physically based runoff/erosion model to study erosional impacts of roads in the study area. Copyright © 2000 John Wiley & Sons, Ltd.

KEY WORDS: rainfall simulation; surface preparation; tropical geomorphology; southeast Asia; soil erosion

INTRODUCTION

During the past 50 years, agriculture has intensified on steep slopes in northern Thailand as ethnic hilltribe groups have migrated southward and mountain population densities increased. Unpaved road networks have also recently developed in these areas. As is the case with unstable agricultural practices, roads can substantially disrupt drainage basin hydrology and geomorphology. The impacts of these two activities are not well understood, and the cumulative watershed effects of roads versus agricultural activities have yet to be quantified satisfactorily. In two prior works in northern Thailand, we have demonstrated that rural roads potentially disrupt hydrologic and erosional processes disproportionately to their areal extent, compared with agriculture-related lands in a tropical mountainous watershed (Ziegler and Giambelluca, 1997a,1997b). These findings represent a foundation to investigate the problem in detail. The objectives of this paper are: (1) to use rainfall simulation to quantify runoff generation and sediment transport on roads, footpaths and

* Correspondence to: Dr A. D. Ziegler, Department of Geography, University of Hawaii, 2424 Maile Way 445, Honolulu, HI 96822, USA. E-mail: adz@hawaii.edu
Contract/grant sponsor: National Science Foundation; contract/grant number: 4923-92
Contract/grant sponsors: Environmental Protection Agency; Horton Hydrology (AGU)

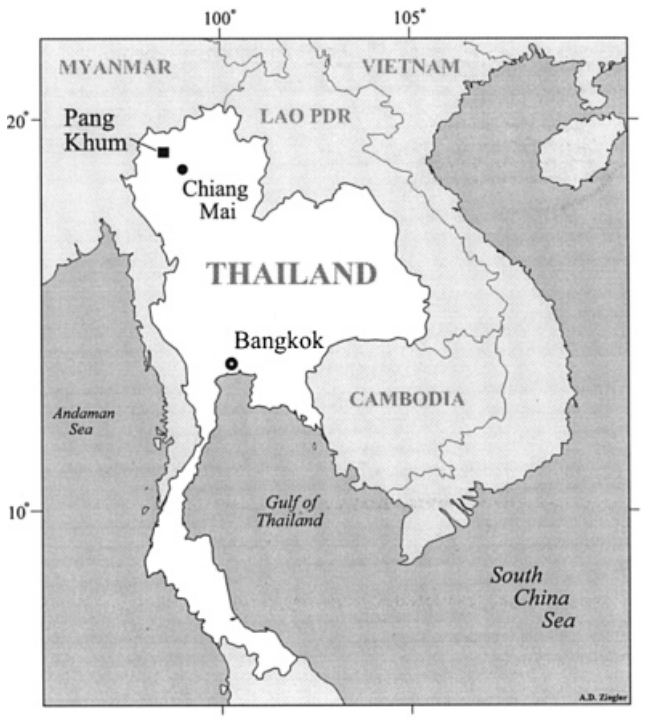

Figure 1. All work was performed near Pang Khum village in northern Thailand

agricultural lands; and (2) to compare data from small plot rainfall simulation experiments on roads with those from a natural rainfall event on a larger-scale road plot. The work focuses on the Horton overland flow (HOF) runoff mechanism because interception of subsurface flow by roads is rare in the study area.

STUDY AREA

The study site is near Pang Khum village (19°3′N, 98°39′E), within the Samoeng District of Chiang Mai Province, *c*. 60 km NNW of Chiang Mai, Thailand (Figure 1; included in the Sam Mun study area reported in Ziegler and Giambelluca, 1997a,1997b). The area has a monsoon rainfall regime with a rainy season extending from mid-May to November, during which *c*. 90 per cent of the 1200–1300 mm annual rainfall occurs. All work was performed within the 93·7 ha Pang Khum Experimental Watershed (PKEW; Figure 2). Bedrock material is Triassic granite (field observation; Hess and Koch 1979). Highland soils in northern Thailand are largely Oxisols and Ultisols associated with deeply weathered regolith; shallow Inceptisols, and Ultisols are less abundant (adapted from FAO classification in Kubiniok, 1992). PKEW soils appear to be Ultisols, Alfisols and Inceptisols (J. Pintong, Soil Survey, Faculty of Agriculture, Chiang Mai University, personal communication). Soil properties determined on the Lower PKEW Road and adjacent fallow fields are listed in Table I.

Roads constitute <1 per cent of the PKEW area. Approximately 27 per cent of the basin area is agricultural land (active upland/paddy or recently fallow); 72 per cent is disturbed, primary hardwood forest or advance secondary vegetation; and <1 per cent is occupied by dwelling sites (adapted from Fox *et al.*, 1995). The original pine-dominated forest has been altered by hundreds of years of swidden cultivation by Karen, Hmong and recently Lisa ethnic groups. Most lower basin slopes are cultivated by Lisu villagers who migrated to Pang Khum from Mae Hong Son Province *c*. 20 years ago. The farming system now resembles a long-term cultivation system with short fallow periods, as opposed to traditional Lisu long fallow practices (cf. Schmidt-Vogt, 1998). Major crops include upland rice, corn, cabbage, onions, flowers, fruit and some paddy rice.

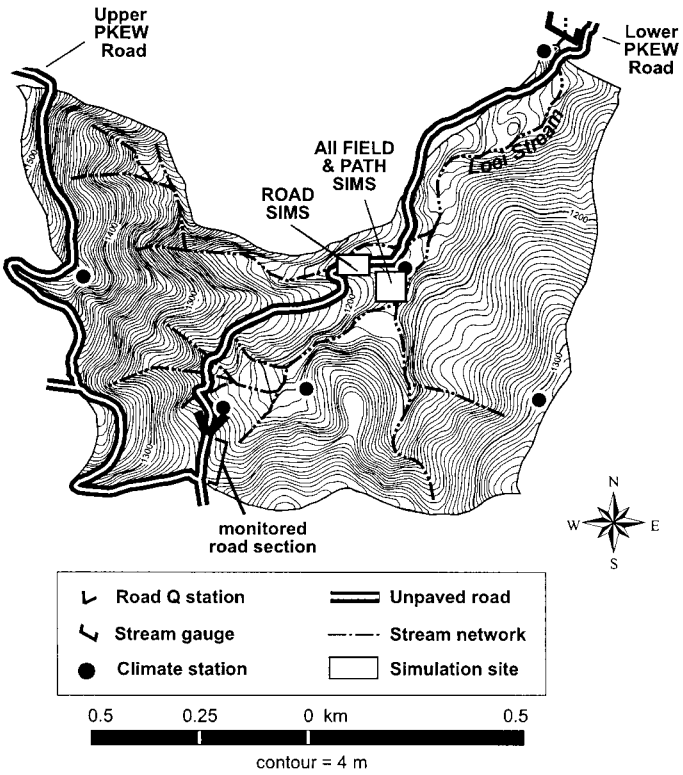

Figure 2. The 93·7 ha Pang Khum Experimental Watershed (PKEW). White boxes identify locations of the ROAD simulations on the Lower PKEW Road and the agriculture-related and footpath simulations in the upland rice field

Opium was an important crop before government eradication began about 10 years ago. The Upper and Lower PKEW Roads are important sediment sources for material entering the stream channel network (Figure 2). At the beginning of the rainy season loose road surface material accumulated during the dry season is flushed by surface flow during the first few rainstorms. Thereafter, light daily traffic (*c*. four motorcycles and two trucks per day) detaches more sediment and creates ruts for gully initiation. Filling of gullies with unconsolidated material is an additional source of easily eroded material. Because HOF is frequently generated on roads (Ziegler and Giambelluca, 1997a), surface runoff continually transports sediment and incises concentrated flow channels throughout the wet period. During the largest rain event of 1998 (STORM, discussed below), HOF from the 1650 m Lower PKEW Road constituted 10 per cent of the basin storm hydrograph for the first hour. Because road runoff exit points tend to be where the road intersects stream channels, conveyance efficiency to the stream network is *c*. 75 per cent (based on field survey).

METHODOLOGY

Simulation treatments

In February of the 1998 and 1999 dry seasons, 27 rainfall simulations were performed on a 50 m road section and five other surfaces within an upland rice field, including (1) hoed field, (2) upland field, (3) basin access path, (4) field maintenance path and (5) fallow field. The rice field, consisting of 0·25 to 0·50 m rice stubble at the time of fieldwork (40–60 per cent standing cover), was harvested in November 1997. Prior to simulation, the field was burned in a manner consistent with typical practice, except earlier in the season. A

Table I. Soil properties on and adjacent to the road surface at PKEW

Descriptor/Property	Units	Road surface*	Road sediment*	Upland field*
Sand fraction	%	54·4 ± 4·9	57·3 ± 8·2	57·1 ± 5·0
Silt fraction	%	24·0 ± 2·2	22·2 ± 3·8	21·2 ± 4·6
Clay fraction	%	21·7 ± 5·5	20·5 ± 5·5	22·0 ± 4·6
Dominant clay mineral	–	kaolinite†	–	kaolinite†
Particle density	Mg m^{-3}	2·55 ± 0·05	–	2·47 ± 0·06
$pH_{(1:5\ water)}$	–	4·9 ± 0·2	4·8 ± 0·3	5·6 ± 0·5
Organic carbon	%	2·5 ± 0·7	1·6 ± 0·6	3·5 ± 0·9
Total nitrogen	%	0·14 ± 0·03	0·13 ± 0·03	0·24 ± 0·03
Potassium	mg kg^{-1}	134 ± 68	319 ± 131	382 ± 118
Cation exchange capacity	cmol kg^{-1}	9·8 ± 2·6	–	14·7 ± 2·2
Calcium	cmol kg^{-1}	5·4 ± 3·1	–	16·3 ± 9·9
Magnesium	cmol kg^{-1}	0·58 ± 0·40	–	1·16 ± 0·52
Sodium	cmol kg^{-1}	0·14 ± 0·07	–	0·30 ± 0·09
Phosphorus	cmol kg^{-1}	0·34 ± 0·23	–	0·99 ± 0·32
Exchangeable bases	%	63·1 ± 19·8	–	96·5 ± 8·9

* Road surface and upland field values were taken from four to eight 90 cm^3 surface cores; road sediment values were derived from sediment output of the eight ROAD simulations; values are ± one standard deviation.
† In addition to moderate amounts of kaolinite, PKEW mineralogy also includes traces of illite, vermiculite, gibbsite, montmorillonite and chlorite.

portion of the burned field was tilled with a traditional hand-held hoe. The upland field treatment was the unhoed burned field (*c*. 90 per cent bare ground). The 0·15 m (W) basin access path, used daily by 10 to 20 farmers, is the primary walking entry way into lower PKEW. The 0·14 m (W) field maintenance paths were created on the hoed surface by three Lisu farmers, wearing sandals, traversing up and then down a line 31 times. The fallow field consisted of <0·5 m tall grasses and shrubs (*c*. 80 per cent standing cover). Hereafter, simulation surfaces are referred to as ROAD, HOED FIELD, UPLAND FIELD, PATH, FIELD PATH and FALLOW FIELD (Table II).

Measurement of physical properties

Prior to rainfall simulation, soil physical properties for each plot were measured either 1 m below or above the simulation plot. Surface bulk density (ρ_b) and antecedent soil moisture (Θ_n) were determined by sampling the upper 5 cm with a 90 cm^3 core ($n \geq 3$ for each plot), then oven drying for 24 h at 105° C. Subsurface bulk densities were determined similarly at 5 and 10 cm depths. Soil penetrability, a measure of the ease with which an object can be pushed into the soil (cf. Bradford, 1986), was measured with a static Lang™ penetrometer (Gulf Shores, AL). The penetrometer provides an index of normal strength, termed penetration resistance (PR), for the upper soil surface, typically *c*. 0·5 cm in depth. Plot slope angles were determined with an Abney level. Saturated hydraulic conductivity (K_s) was estimated from infiltration measurements taken *in situ* with Vadose Zone Equipment Corporation (Amarillo, TX) disc permeameters. Use of this instrument in PKEW is explained by Ziegler and Giambelluca (1997a).

Rainfall simulator and plot design

The rainfall simulator consisted of two vertical, 4·3 m risers, each directing one 60° axial full cone nozzle (70 μm orifice diameter) toward the surface. Water from a refillable storage container (1850 l minimum) was fed to the simulator through 2·5 cm diameter PVC hose by a 750 W centrifugal pump and a 2·5 kW gasoline-powered generator at 172 kPa (25 psi). This operating pressure produces rainfall energy flux densities (EFDs) of 1700–1900 J m^{-2} h^{-1}, which approximates energies sustained for 10–20 min during the largest annual PKEW storms (based on preliminary analysis of 2 years of rainfall data). Tubular, sand-filled, geotextile bags (3·0 m × 0·2 m × 0·1 m) were arranged to form rectangular plots. The bags were created from low permeability LINQ GTF 200 geotextile. Plot dimensions are shown in Table II. Within PATH and FIELD PATH plots, the compacted path surface occupied only *c*. 18 and 16 per cent of the respective areas; the remaining

Table II. Mean slope, antecedent soil mass wetness (w), rainfall intensity (R_i) and energy flux density (EFD) for rainfall simulation experiments

Treatment	n	Plot dimensions (m)	Slope (m m^{-1})	w (g H_2O/g dry soil)	R_i (mm h^{-1})	EFD (J m^{-2} h^{-1})
ROAD	8	3·75 × 0·85	0·15 ± 0·02 a*	0·12 ± 0·03 b	105 ± 10 a	1774 ± 175 a
HOED FIELD	4	3·25 × 0·85	0·23 ± 0·02 b	0·06 ± 0·01 a	110 ± 13 a	1753 ± 218 a
UPLAND FIELD/PATH	7	3·25 × 0·85†	0·20 ± 0·02 b	0·05 ± 0·01 a	107 ± 10 a	1818 ± 177 a
FIELD PATH	4	3·25 × 0·85	0·21 ± 0·02 b	0·06 ± 0·01 a	105 ± 15 a	1807 ± 262 a
FALLOW	4	3·25 × 0·85	0·32 ± 0·02 c	0·04 ± 0·01 a	97 ± 7 a	1634 ± 125 a

* Column values with same letter are *not* statistically different (ANOVA B-D, $p = 0{\cdot}05$); values are ± one standard deviation.
† PATH plot length is 3·75 m

surfaces were similar to UPLAND FIELD and HOED FIELD, respectively. Non-path surfaces were included within path treatments to investigate sediment transport from the entire 'path complex', i.e. erodible non-path surfaces of relatively high infiltrability juxtaposed with compacted path surfaces that frequently generate HOF.

At the base of all plots, geotextile bags were aligned such that runoff was funnelled into a shallow drainage trench. A V-shaped aluminium trough, inserted into the vertical trench wall, allowed event-based sampling. On non-road plots, the trench face and triangular surface area immediately above the outlet were treated with a 5:1 mixture of water and Soil Sement™ (an acrylic vinyl acetate polymer from Midwest Industrial Supply, Inc., OH) to prevent sediment detachment on these non-plot areas. The *c*. 0·21 m^2 triangular area (in addition to plot areas above) contributed runoff, but not sediment. Rainfall was measured for 40 to 50 min with manual gauges placed on the plot borders. The plot design is shown in Figure 3. Energy flux density (J m^{-2} h^{-1}) of simulated rainfall was calculated as:

$$EFD = \frac{R_i}{V_{D_{50}}} \frac{m\nu^2}{2} \tag{1}$$

where R_i is event rainfall intensity (m h^{-1}); V_{D50} is the volume (m^3) of the median-diameter (D_{50}) raindrop, determined by:

$$V_{D_{50}} = \frac{4}{3}\pi\left(\frac{D_{50}}{2}\right)^3 \tag{2}$$

In Equation 1, m is the mass (kg) of the D_{50} drop, which is estimated as

$$m = (\rho_w - \rho_{air})V_{D_{50}} \tag{3}$$

where ρ_w and ρ_{air} are 1000 kg m^{-3} and 1·29 kg m^{-3}, respectively. Factor ν in Equation 1 is the fall velocity (m s^{-1}) of the D_{50} drop, determined by the equation (from Best, 1950):

$$\nu = V_{\max}\left(1 - e^{-\left(\frac{D_{50}}{b}\right)^{\beta}}\right) \tag{4}$$

with $V_{\max} = 9{\cdot}5$ (m s^{-1}), $b = 1{\cdot}77$ and $\beta = 1{\cdot}147$ (from Mualem and Assouline, 1986). Median drop size was estimated from nozzle manufacturer engineering data. Rainfall EFD is more informative than rainfall intensity because terminal velocity and drop size distributions from rainfall simulators differ from those of

Figure 3. Rainfall simulation plot design shown during one simulation. The bases of the vertical simulator risers rest on the elevated bench to the right of the two subplots. White bottles are used for measuring rainfall intensity. Water flows from the plots into shallow collection trenches at the plot outlet

natural rainfall. Additionally, simulators with the same rainfall intensity, but different architectures, will have different EFDs.

Simulation data collection and calculations

Time to runoff (TTRO) was recorded during each event. Runoff samples were collected at TTRO, then again at 2·5, 5 or 10 min intervals afterwards. Most simulations were conducted for 60 min after TTRO (except when limited by water supply); PATH simulations were conducted for only 45 min. Discharge was determined by measuring the time to fill of a 525 ml bottle. After settling, the supernatant was decanted and discharge samples were oven dried at 105°C for 24 h to determine mass of material transported. Sample discharge volumes were reduced to account for the presence of sediment. Instantaneous concentrations (C_t) were calculated as sediment mass per corrected discharge volume. Instantaneous discharge and sediment output values were adjusted to rates per unit area by dividing by filling time and plot area (plot areas for sediment and discharge calculations were different, see above). The rates were then divided by EFD values. Normalized instantaneous discharge (Q_t) and sediment output (S_t) therefore have units $m^3\ J^{-1}$ and $kg\ J^{-1}$, respectively. Cumulative discharge (Q_{cum}) was calculated as total plot runoff volume prior to any time t, divided by EFD since TTRO. Calculated slightly differently, cumulative sediment (S_{cum}) output was total sediment mass at time t divided by EFD since the beginning of the simulation. Values were normalized differently because EFD prior to TTRO contributes differently to subprocesses controlling runoff generation and sediment transport, i.e. at the beginning of rainfall, sediment is detached by raindrop impact and material is transported downslope via rainsplash. In essence, energy prior to TTRO contributes to the sediment supply that will be transported throughout the event after runoff commences. With discharge, rainfall is infiltrated, then ponded, before HOF generation. Only by contributing to surface sealing, which may speed up runoff generation, does energy prior to TTRO contribute to all-event discharge. Total normalized event discharge and sediment output are referred to as Q_{event} and S_{event}.

Measuring road discharge during natural events

To compare ROAD simulation data with discharge and sediment transport data from natural runoff events, we constructed a discharge collection station at the footslope of a 165 m road section near the watershed mouth (Figure 2). A trench was dug across the road to a depth and width of *c*. $0{\cdot}5 \times 0{\cdot}75$ m. Vertical trench walls were reinforced with 4 mm steel. Depressions in the transitional area between the road surface and the reinforced walls were filled with concrete to prevent incision. The trench bottom was covered with corrugated aluminium roofing, which was shaped in a semicircle and sloped (10 per cent) to minimize sedimentation

Table III. Mean compaction- and infiltration-related variables* for the six simulation surfaces

Treatment	$\rho_{b(0–5\ cm)}$ (Mg m^{-3})	$\rho_{b(5–10\ cm)}$ (Mg m^{-3})	$\rho_{b(10–15\ cm)}$ (Mg m^{-3})	PR (MPa)	K_s (mm h^{-1})
ROAD	1·45 ± 0·13 (74) b	1·36 ± 0·11 (16) a	1·35 ± 0·10 (16) a	6·4 ± 0·4 (160) d	15 ± 9 (26) a
PATH	1·40 ± 0·11 (21) b	1·37 ± 0·09 (3) a	1·32 ± 0·14 (3) a	6·4 ± 0·7 (90) d	8 ± 5 (6) a
FIELD PATH	1·24 ± 0·11 (22) a	1·25 ± 0·16 (4) a	1·28 ± 0·12 (4) a	2·8 ± 1·1 (40) b	244 ± 88 (10) b
UPLAND FIELD	1·20 ± 0·09 (36) a	1·25 ± 0·15 (5) a	1·23 ± 0·13 (5) a	4·7 ± 1·4 (98) c	133 ± 77 (6) b
HOED FIELD	1·19 ± 0·06 (22) a	1·22 ± 0·03 (4) a	1·30 ± 0·07 (4) a	1·8 ± 1·2 (40) a	316 ± 129 (10) b
FALLOW FIELD	1·11 ± 0·05 (6) a	na	na	1·7 ± 0·9 (60) a	129 ± 38 (6) b

* ρ_b is bulk density at indicated depth; PR is penetration resistance; K_s is saturated hydraulic conductivity; values are ± one standard deviation; values in parentheses are sample sizes; values in each column with the same letter are *Not* statistically different (ANOVA B-D, $p = 0·05$)

during events. The trench was covered by a perforated steel grate to accommodate traffic. A tipping bucket rain gauge (0·254 mm threshold) and datalogger were used to measure 1 min rainfall intensities at the site. An 'average' road cross-section was composed of *c*. 1·9 m of compacted track and 1·3 m of less compacted surface; this 3·2 m width represents the surface commonly travelled upon by vehicle (automobile and motorcycle), pedestrian and animal traffic. Tracks were occasionally incised 5–15 cm. Non-track surfaces often contained vegetation. Slopes for consecutive 20 m intervals starting at the trench were 0·12, 0·23, 0·25, 0·18, 0·09, 0·07, 0·11 and 0·12 m m^{-1}. Discharge and sediment output values were measured similarly to those in the ROAD simulations. Values were divided by filling time, contributing area (3·2 m × 165 m), and event EFD, which was calculated using raindrop size data from Baruah (1973) and Equations 1–4.

Data analysis

Because simulation durations occasionally differed, most data were analysed based on simulation times of 45 min. The lone HOED FIELD simulation producing runoff was conducted for only 25 min following TTRO. Because there was no replication, HOED FIELD was not included in statistical analysis. Similarly, FALLOW FIELD was not included because none of the four replications produced runoff. All data were analysed, after $\log_{10}$ transformation, using one-way analysis of variance (ANOVA), followed by post-hoc multiple comparison testing with the Bonferroni/Dunn test (B-D) when the *F*-values were significant at $p = 0·05$ (Gagnon *et al.*, 1989). On compacted ROAD and PATH surfaces, *c*. 62 per cent of the 250 PR values reached a maximum value of 6·7 MPa; rarely was the maximum reached on other surfaces. The distributions of road and path PR values were therefore truncated. Bounded data usually require special statistical treatment, but because ROAD and PATH data were substantially higher than those of the other surfaces, and we do not focus on differences between these two treatments, the use of ANOVA is justified. The non-parametric Spearman rank correlation coefficient (r_s) was used to evaluate the relationship between compaction indices (PR and ρ_b) and TTRO data.

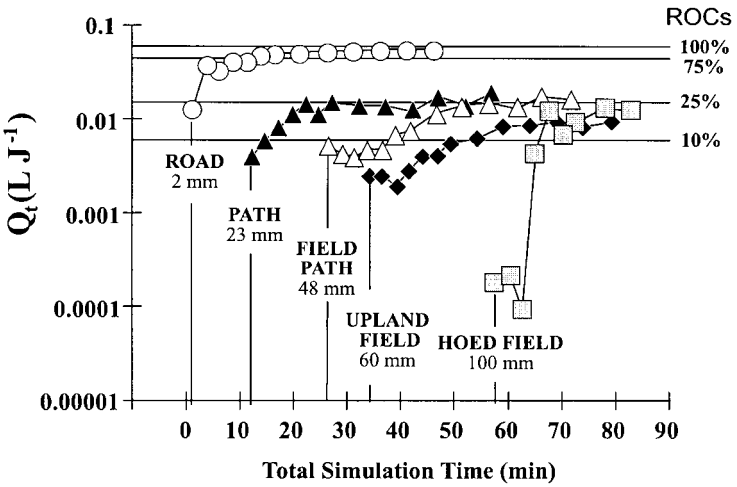

Figure 4. Normalized instantaneous discharge (Q_t) plotted since the beginning of rainfall simulation. Values are normalized by rainfall energy flux density (EFD) and plot area. Data series begin at mean time to runoff (TTRO). Values below surface identifiers refer to rainfall depths falling on the plot before TTRO. Runoff coefficients (ROCs) are based on rainfall intensity data for all simulations. HOED FIELD has no replication, as only one of four events produced runoff. FALLOW FIELD (not shown) did not produce runoff

RESULTS

Compaction indices

ROAD and PATH surfaces had statistically higher $\rho_{b(0–5\ cm)}$ and PR values, compared with the other surfaces ($p = 0{\cdot}05$; Table III). FIELD PATH, UPLAND FIELD, HOED FIELD and FALLOW FIELD had surface ρ_b values that were statistically indistinguishable. ROAD and PATH surfaces had the highest PR values (means *c*. 6·4 MPa); HOED FIELD and FALLOW FIELD were the least compacted surfaces by this measure (<2·0 MPa). Compaction on roads and paths extended down to at least 15 cm, although subsurface values were not statistically different from those of the other surfaces.

Instantaneous discharge and time to runoff

Figure 4 shows instantaneous discharge (Q_t) and other related runoff data for the simulation surfaces. Each data point is a mean of all simulations producing runoff. Each series begins at its mean TTRO. To indicate the proportion of rainfall transported from the plots as discharge, runoff coefficients (ROC = discharge volume/rainfall volume × 100 per cent) based on mean rainfall data from all simulations are shown. Values below treatment identifiers represent rainfall depths falling on the plot before TTRO. Road surface runoff response stands out, with mean TTRO occurring in just a little more than 1 min. ROAD Q_t exceeded 75 per cent of rainfall after *c*. 15 min (total event ROC was >80 per cent). In marked contrast, FALLOW FIELD did not produce runoff after 60 min of simulated rainfall during four events; HOED FIELD produced runoff in only one of four events. TTRO for the lone HOED FIELD runoff event was 58 min, after *c*. 100 mm had fallen on the plot surface. TTRO was unique for all other surfaces, with runoff occurring first on PATH, then FIELD PATH, and finally UPLAND FIELD. Non-road instantaneous ROC values were typically <25 per cent; FIELD PATH ROC was consistently <15 per cent.

Sediment output

Following preliminary analysis of sediment transport data, UPLAND FIELD ($n = 4$) and PATH ($n = 3$) treatments were combined into one group. Slope, antecedent soil moisture, rainfall intensity and event EFD

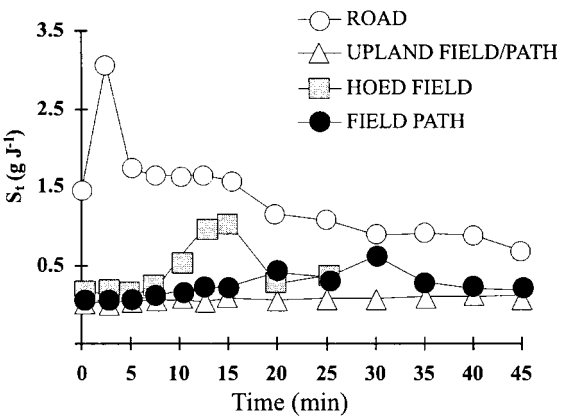

Figure 5. Normalized instantaneous sediment output (S_t) did not produce runoff. The HOED series has no replication; FALLOW FIELD (not shown) did not produce runoff

Table IV. Mean runoff and sediment transport data* for rainfall simulation experiments producing runoff

Treatment	*n*	TTRO (min)	Q_{TTRO} (ml J^{-1})†	Event ROC (%)	S_{event} (g J^{-1})	C_{event} (kg m^{-3})
ROAD	8	1·1 ± 0·3 a†	48 ± 10 c	80 ± 6	1·23 ± 0·54 c	23 ± 10 b
HOED FIELD	1	57·8 –	7 –	5 –	0·11 –	50 –
UPLAND FIELD/PATH	7	20·3 ± 8·5 b	13 ± 3 b	14 ± 5	0·05 ± 0·02 a	5 ± 2 a
FIELD PATH	4	34·1 ± 12·8 b	6 ± 2 a	6 ± 3	0·14 ± 0·09 b	35 ± 14 b

* Q_{TTRO} is total discharge normalized by rainfall energy flux density (EFD) since runoff initiation; S_{event} is total sediment output normalized by EFD since beginning of simulated rainfall; C_{event} is total event concentration calculated from original data.
† Values in a column with the same letter are *Not* statistically different (ANOVA B-D, $p = 0{\cdot}05$); dash denotes treatment was not included in statistical analysis because $n = 1$; values are ± one standard deviation.

for the five remaining surface groups are summarized in Table II. Table IV lists mean values of TTRO, normalized total discharge, event ROC values, normalized total sediment output, and event sediment concentration for groups producing runoff. ROAD instantaneous sediment transport (S_t) values were often one order of magnitude higher than those of other surfaces (Figure 5). ROAD (S_t) was characterized by an output peak within the first few minutes after TTRO, followed by a gradual decline throughout the remainder of the simulation. The response peak is related to flushing of easily transported, loose surface material. Normalized event sediment output was likewise an order of magnitude higher on the ROAD treatment (Table IV). Sediment transport for the other surfaces was initially very low following TTRO, with UPLAND FIELD/PATH values remaining relatively low for the entire simulation (Figure 5). HOED FIELD and FIELD PATH surfaces, however, experienced small output peaks, suggesting detached material was available for transport on these recently worked surfaces, once surface runoff reached sufficient depth and shear stress. Irregular discharge during the HOED FIELD resulted from (1) windy conditions, which limited rainfall falling on the plot surface, and (2) a very rough surface, on which creation and destruction of flow-blocking microdams occurred. Low UPLAND FIELD/PATH S_t values are related to limited loose sediment on these surfaces and to high shear strength of the surface crust existing on the rice field, from which the plots were created.

Sediment concentration

In general, ROAD produced relatively high sediment output from relatively large runoff volumes (Figure 6a). ROAD instantaneous sediment concentrations (C_t) were initially *c*. 100 g l^{-1}, but fell over time as loose

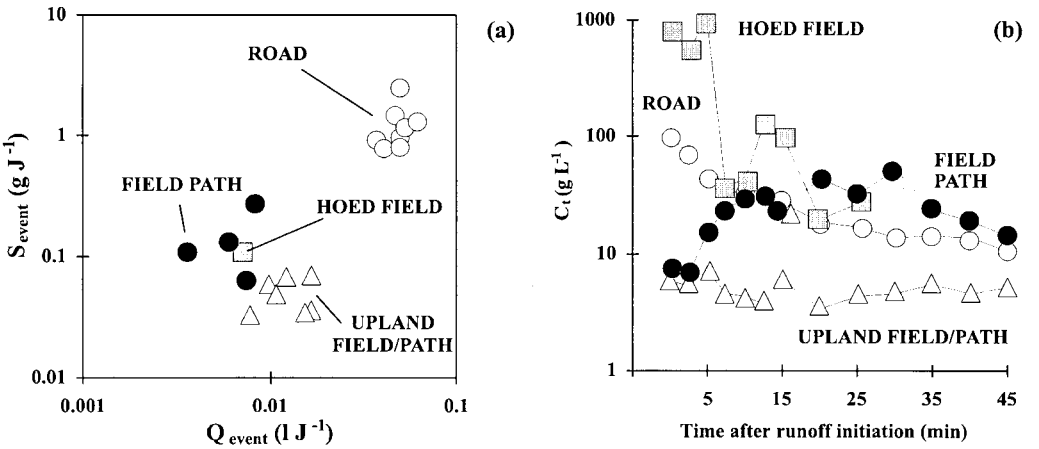

Figure 6. (a) Normalized event sediment output (S_{event}) versus normalized event discharge (Q_{event}). Sediment values were normalized by rainfall energy flux density (EFD) since the beginning of the simulation; discharge values were normalized by the energy since runoff initiation. (b) Instantaneous sediment concentration for four groups of simulation surfaces. In both panels, HOED has no replication; FALLOW FIELD did not produce runoff (not shown)

material was flushed from the surface (Figure 6b). In comparison, the other surfaces produced less total sediment from smaller volumes of runoff (Figure 6a). Owing to low discharge, HOED FIELD and FIELD PATH C_t values were at times the highest of all events; and total event concentrations for these surfaces were greater than those of ROAD (Table IV). However, sediment output from these surfaces was minimal (Figure 5). Although more replications are needed to understand sediment transport on these surfaces clearly, high C_t values are realistic, as hoeing detached a generous supply of loose aggregates and soil particles. Sediment concentration on the UPLAND FIELD/PATH treatments were the lowest of all treatments, again owing to surface resilience on the upland field.

DISCUSSION

Influence of compaction on K_s and runoff generation

Highly compacted surfaces, such as roads and paths, often have low infiltration rates because soil aggregates have been destroyed by compaction and the surface layer may be sealed by fine material. Significant negative correlation existed between K_s and the two compaction indices, $\rho_{b(0-5\ cm)}$ and PR: $r_s = -0{\cdot}668$ ($P < 0{\cdot}0001$) and $r_s = -0{\cdot}821$ ($P < 0{\cdot}0001$), respectively. Penetration resistance was sensitive to thin surface crusts not detectable with the 5 cm ρ_b core. With respect to runoff generation, TTRO showed strong negative correlation with ρ_b and PR: $r_s = -0{\cdot}766$ ($P = 0{\cdot}0008$) and $r_s = -0{\cdot}753$ ($P = 0{\cdot}0010$), respectively. TTRO could be well predicted using step-wise regression from $\rho_{b(0-5\ cm)}$ and PR data: $R^2 = 0{\cdot}822$ ($P < 0{\cdot}0001$). Correlation between compaction indices and infiltration-related phenomena suggest that easily obtained ρ_b and PR data can be used to extrapolate K_s and TTRO data sets, when sufficient experimentation is prohibited by time restraints or physically unfavourable conditions (e.g. steep slopes). The above correlations may change under wetter experimental conditions, as PR and TTRO are dependent on soil moisture.

Comparing HOED FIELD and FIELD PATH compaction and TTRO data is informative because the path treatment was created on the hoed surface. One research hypothesis was that compaction from walking would enhance HOF generation on the FIELD PATH treatment. The small number of passes during dry antecedent moisture conditions increased $\rho_{b(0-5\ cm)}$ by <5 per cent, but significantly increased PR from 1·8 to 2·8 MPa

(Table III). Additionally, K_s was reduced by 23 per cent as foot traffic destroyed most large aggregates and clods. Using the bulk density methodology, we could not detect the shallow compaction on the hoed surface, but the resulting thin mechanical crust was detectable using the penetrometer and disc permeameter. In terms of runoff generation, the foot traffic increased runoff generation: TTRO occurred after *c*. 34 min of rainfall during all four FIELD PATH events, compared with no runoff generation after 90+ min on three of the four HOED FIELD simulation experiments.

Erosion on path complexes

Juxtaposition of compacted footpaths with more erodible planting surfaces could result in substantial surface erosion if sufficient HOF is generated on the path surfaces. TTRO data in Figure 4 support enhanced runoff generation on the path surfaces, i.e. PATH<UPLAND; FIELD and FIELD; PATH<HOED; FIELD. Again, the compacted surface of PATH and FIELD PATH constituted < 20 per cent of the simulation surface; the remaining surface was similar to UPLAND FIELD and HOED FIELD, respectively. The intention of including both path and non-path surfaces in simulation plots was to investigate the interaction of path-generated HOF with the erodible agricultural surface. For the two path treatments, runoff was initiated on the path portion of the simulation plot, and occurred on most of the PATH plot by the end of simulation. The non-path portion of FIELD PATH did not contribute noticeably to runoff. Had 'path' surfaces comprised the entire plot, TTRO would certainly have decreased and runoff would have increased for both treatments, as K_s on the compacted portion of the plots was lower than that of the field portion by 80–120 mm h^{-1} (Table III).

Sediment transport was not substantial for either path treatment (Table IV, Figure 5), because (1) little HOF was generated on FIELD PATH (Event ROC < 15 per cent), and (2) the non-path surface of PATH had high shear strength (PR = 4·7 MPa), thereby resisting detachment/entrainment by path-generated HOF. Concentration data (Figure 6a) support the potential for high sediment transport on complexes resembling FIELD PATH if sufficient HOF is generated. For example, FIELD PATH C_t values were the highest of all treatments *c*. 20 min after TTRO (Figure 6b), and relatively high S_{event} was generated from low discharge volumes (Figure 6a). Some sediment output was non-path material entrained by on-path flow. Although walking impact enhanced runoff generation, it did not increase surface shear strength enough to resist hydraulic erosion. The path surface was susceptible to micro-rill incision and headward expansion as knick points migrated upslope (cf. flume studies of Bryan and Poesen, 1989; Merz and Bryan, 1993). Decreases in sediment output after *c*. 30 min runoff may be related to armouring. The hydrological behaviour of the 'artificial' NEW PATH surface may not represent compacted field paths that evolve over the course of a growing season. We have recently found these 'older' paths to have ρ_b, PR and K_s values more similar to those of the PATH rather than NEW PATH. Thus, runoff generation may be better represented by the PATH treatment. If this is the case, and sediment output is similar to FIELD PATH, the potential for significant sediment transport exists.

Surface preparation and sediment transport

PKEW road surfaces have high sediment production rates in part because relatively high discharge volumes flush readily available, loose surface sediment. Discharge is high because road surfaces are highly compacted, thus infiltrability is low, and a large percentage of rainfall becomes runoff (Ziegler and Giambelluca, 1997a). Loose sediment is made available by 'surface preparation' processes occurring between and during storms (cf. Bryan, 1996). Surface preparation is any process that influences the availability, erodibility/detachability or transport of surface material. For example, vehicle traffic is a principal mechanism detaching sediment both during dry and wet periods. Additionally, some sediment entrained during runoff events is redistributed on the road surface, and is available for transport during the next overland flow event. Although non-road surfaces also undergo various surface preparation processes, surface runoff is more rare. Furthermore, vehicle detachment on roads is a daily phenomenon; preparation processes on other lands occur less frequently. For example, weeding on agricultural lands, which breaks up crusted/compacted surfaces, may occur only a few times during the rainy period. Hoeing may occur only once annually.

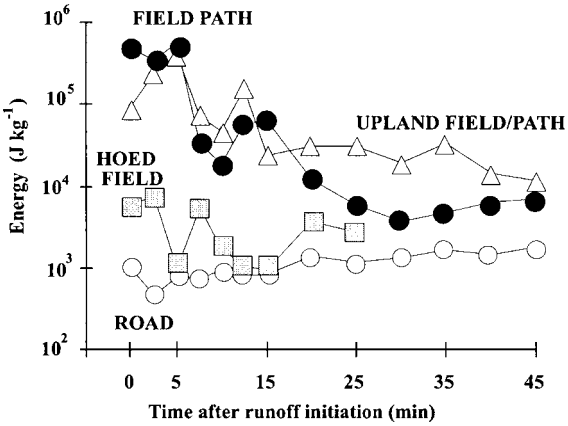

Figure 7. Energy required to remove 1 kg of sediment from the simulation plots. Removal energy for ROAD is relatively low, owing to high volume, high velocity discharge flushing easily entrainable sediment on the road surface. The HOED has no replication; FALLOW FIELD (not shown) did not produce runoff

Under dry antecedent soil moisture conditions, substantial sediment transport from PKEW agricultural surfaces will require significant rainfall depth (either as one large event, or as a series of showers that shorten TTRO by increasing soil moisture content) to generate sufficient HOF. Much less rainfall energy is required to generate runoff and remove loose surface material from roads. Figure 7 shows instantaneous rainfall energy needed to remove 1 kg of sediment from the small-scale simulation plots (J kg^{-1}; after Sutherland *et al.*, 1996). ROAD has the lowest values, with agricultural surfaces typically being much higher. If rainfall prior to TTRO were included in this calculation, non-road values would substantially increase, particularly those for the one HOED event that required *c.* 60 min of rainfall (EFD $\approx$ 1700 J m^{-2} h^{-1}) to produce runoff. At hillslope scales where roads channel runoff along the surface for great distances, sediment transport can be enhanced by high velocity flow that transports large aggregates and gravel not entrained by lower volume flows, such as those in the plot studies above. Furthermore, during high magnitude storm events, overland flow on long slopes can incise the compact road surface, especially in sections where ruts have already been formed.

Representativeness of the ROAD simulation data

One research goal was to use rainfall simulation data to assign parameters in KINEROS2 (Smith *et al.*, 1995), a physically based model that will be used to describe hillslope runoff and erosion processes. Simulation data, obtained at a small scale, must therefore be representative of larger-scale natural phenomena, when normalized similarly. To assess this representativeness, we compared ROAD Q_t and C_t with that collected at the road discharge collection station during several rainstorms. This comparison is shown in Figure 8 for the rainstorm that most closely resembled the simulated events, both in intensity and duration (referred to hereafter as STORM). Rainfall intensities (Figure 8c) are plotted with respect to individual TTRO values (time 0). Simulated rainfall begins *c.* 1 min before TTRO. During the natural event, rainfall was first recorded 24 min before TTRO, with surface saturation, ponding, and 'interplot' HOF also occurring well before runoff initiation. STORM rainfall intensity was highly variable compared with near-constant simulated rainfall intensity. During the high-energy portion of STORM (0–30 min), mean rainfall intensity (89 mm h^{-1}) was only slightly lower than the simulation rate of *c.* 105 mm h^{-1}. However, EFD was substantially higher for STORM (*c.* 2640 vs. 1775 J m^{-2} h^{-1}), owing to median raindrop size being *c.*50 per cent larger than that of simulated rainfall.

Normalized ROAD and STORM Q_t were comparable during the first 30 min following TTRO when the natural rainfall rates were highest. Although falling limbs of the discharge hydrographs appear different, they

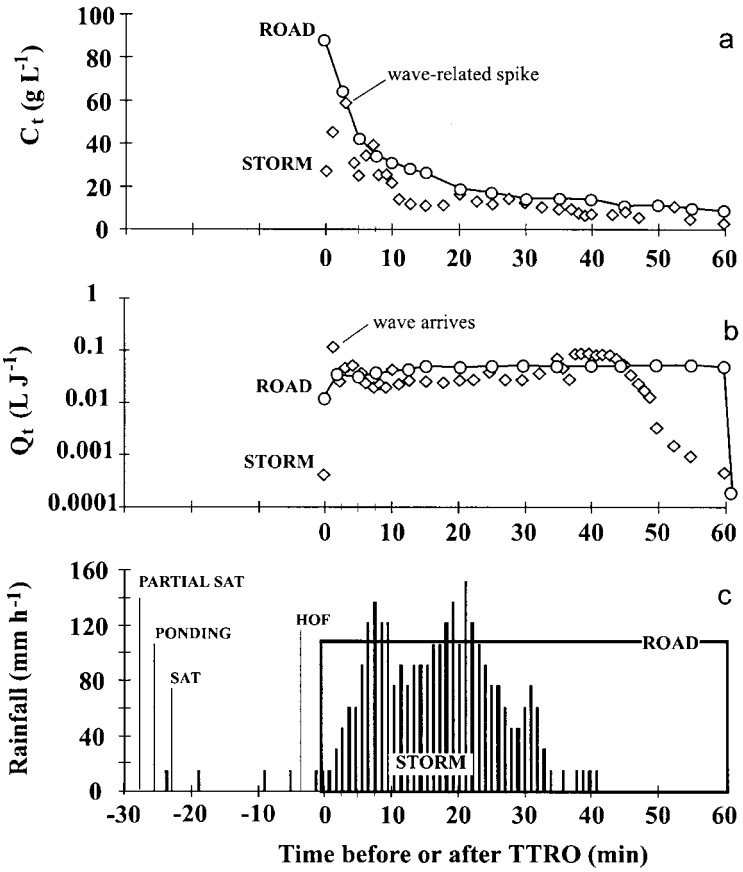

Figure 8. Comparison, for simulated (ROAD) and a natural event (STORM, on a 165 m slope segment), between: (a) sediment concentration (C_t); (b) instantaneous discharge (Q_t); and (c) rainfall intensities. Discharge and sediment-related output data are plotted relative to their individual time to runoff (TTRO). Data from simulation and natural events are normalized similarly. Partial saturation (PARTIAL SAT), ponding, saturation (SAT), and 'interplot' Horton overland flow (HOF) correspond to the natural event

are comparable when differences in plot lengths are considered. After rainfall was discontinued, ROAD plots typically drained in *c*. 0·75 min, equivalent to *c*. 29 min when scaled to the 165 m monitored road section. We stopped measuring the STORM falling limb after 24 min. One critical difference between the two data sets is that at the base of the road section, a 'wave' of runoff water arrived from upslope *c*. 1 min after TTRO (Figure 8b). This phenomenon was not detectable during small-scale ROAD simulations. The STORM C_t spike shortly thereafter (Figure 8c) is associated with the discharge wave, which brings both loose material from upslope and the energy needed to entrain sediment near the plot outlet. Prior to the concentration spike, ROAD C_t was much higher than STORM C_t. Afterwards, ROAD C_t was only slightly higher. Sediment transport decreased at both scales over time as the supply of easily removed surface material became depleted. Post-event observations on the road section indicate that a secondary mechanism contributing to the output decline may have been armouring, as sediment became oriented in crevices of road ruts.

ROAD C_t was higher than that of STORM despite raindrop impact energy and hydraulic energy being greater for the hillslope-scale natural event than for the simulation experiments. ROAD values were higher predominantly because simulations were performed in the dry season when ample loose material had collected on the road surface since the last HOF event several weeks before. STORM was one of a series of wet-season rainshowers that continually depleted surface sediment created by traffic between events. Initial ROAD C_t values (*c*. first 5 min) may be uncharacteristically high to represent wet season phenomena in

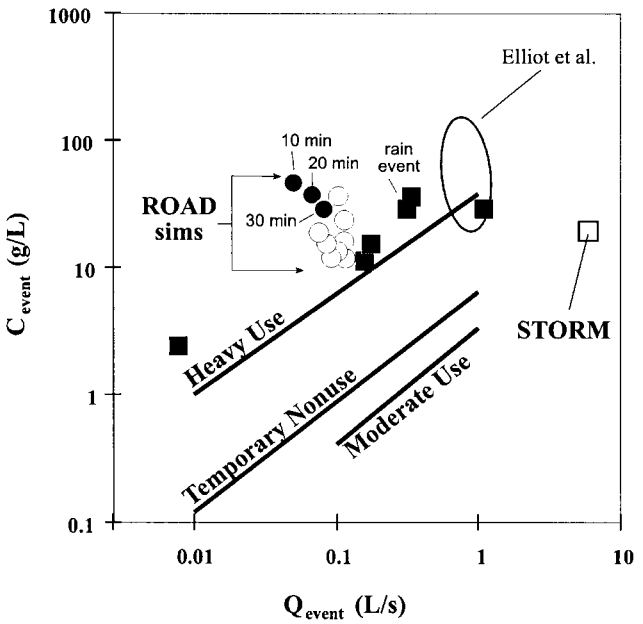

Figure 9. Total 'event' sediment concentration (C_{event}) plotted against total 'event' discharge (Q_{event}) for the ROAD simulations (open circles) and the natural events (squares). Open square is STORM from Figure 8. Mean values occurring at time = 10, 20 and 30 min during ROAD simulations are represented by closed circles. The labelled lines are fitted values determined on roads of varying length during natural events in Washington state, USA, for different levels of traffic (from Reid and Dunne, 1984). The ellipse surrounds 24 values determined in the simulation study of Elliot *et al.* (1995)

general. However, they may be typical of concentrations achieved after long dry periods with frequent traffic or at the beginning of the rainy season before the dry season sediment accumulation is removed.

Comparing ROAD results with other field studies provides another opportunity to assess 'data realism'. Our high initial C_t values are similar to those measured following truck passes in a 40 m^2 simulation plot in New Zealand (30 min, 32–38 mm h^{-1} events) (Coker *et al.*, 1993). When compared with event concentration (C_{event}) and discharge (Q_{event}) data determined from culvert runoff during natural events for 10 road segments in Washington, USA (Reid and Dunne, 1984), our ROAD (open circles) data correspond most closely to roads undergoing heavy usage (Figure 9). Because PKEW roads are lightly used, these comparisons suggests ROAD C_t values are high. However, ROAD values were similar to those of 30 min, 50 mm h^{-1} simulation experiments on *c.* 60 m^2 plots in two western states of the USA (Elliot *et al.*, 1995). The 24 data points encompassed by the ellipse were generated from simulations at eight different sites, varying in soil type, during each of dry, wet and very wet soil conditions. In addition, our simulation values are only slightly higher than those recorded during seven storms on the monitored PKEW road section in August 1998 (solid squares in Figure 9; open square is STORM event of Figure 8). General agreement between simulation and natural event data supports the representativeness of the ROAD simulation data for natural phenomena in PKEW, but reveals limitations of comparing data at different scales. In addition, similar storm events on physically similar road sections could result in substantially different sediment output data if two sites differ in variables affecting erodibility (texture, clay mineralogy, shear strength, organic material, rock content) and/or availability of loose, entrainable material (as affected by age since construction, usage, maintenance activities, mass wasting processes). Our high values, compared with the Reid and Dunne findings on similar slopes, may relate to differences in soil erodibility–although one would surmise that soil originating from the siltstone, sandstone and graywacke bedrock material of the Washington study would be more erodible than the granitic soil in PKEW.

Finally, the STORM value in Figure 9 does not continue the general trend of C_{event} increasing with Q_{event}, as suggested by the Reid and Dunne data (lines) and the lower-volume PKEW rainstorm events (solid squares).

PKEW road surfaces are composed of an erodible surface layer (loose material of limited supply) and a less erodible underlying layer (compacted road surface). After some critical discharge volume has removed the loose material, sediment production diminishes because the underlying surface is resistant to detachment/entrainment.

SUMMARY AND CONCLUSIONS

Rainfall simulation was useful in ascertaining unique differences in runoff generation and sediment transport processes for roads, footpaths and agricultural lands. Roads, having very low saturated hydraulic conductivities, generated runoff quickly (*c*. 1 min) during high intensity events and produced event runoff coefficients >80 per cent. Agriculture-related land surfaces often required very large rainfall depths to produce overland flow when soils were initially dry. Our dry season simulations may understate the importance of agricultural fields to a basin sediment budget, as erosion-producing HOF should occur more frequently under wetter soil conditions. Because of difficulty in generating runoff on agricultural lands, more simulations are needed to better understand overland flow generation and sediment transport on these surfaces. Footpaths, like roads, accelerate runoff, demonstrating their potential to enhance surface erosion by acting as source areas for surface runoff on agricultural lands where Horton overland flow is otherwise rare. However, under our experimental conditions, sediment transport from path complexes was not substantial.

High road discharge volumes flushed loose sediment that had accumulated on the surface between or during rainfall events. Sediment transport on PKEW roads is initially high, then steadily declines over time as loose surface sediment becomes depleted. Sediment output is very sensitive to processes altering the supply of loose surface material, and may be more affected by these processes than by the erodibility of the underlying compacted road surface. If large quantities of surface material are present, such as might occur before the first large wet-season storm, or following any extended dry period, sediment production can be substantial. When compared with discharge and sediment transport on a 165 m road section during natural events, our simulation concentration data are slightly higher. Some caution is therefore needed when validating a physically based runoff/erosion model. Our intention is to parameterize and calibrate the model using small-scale ROAD simulation data, then use natural event data for model validation at the hillslope scales.

ACKNOWLEDGEMENTS

We acknowledge the help of Asu, Ataboo, Atachichi, Aluong (brawn); K. Guntawong (the General); P. and N. Lamu (sharing their home); S. Yarnasarn, Geography, Chiang Mai University; J. F. Maxwell (plant identification); M.A. Nullet (engineering prowess); T.T. Vana (field assistance); the Soil and Land Conservation Division of the Department of Land Development, Bangkok and Chiang Mai offices (soil analyses). This project was partially funded by the National Science Foundation Award (grant no. 4923-92) to T. W. Giambelluca and R. A. Sutherland of the University of Hawaii. Alan Ziegler is supported by an Environmental Protection Agency Star Fellowship and a Horton Hydrology Research Award (Hydrological Section, American Geophysical Union).

REFERENCES

Baruah PC. 1973. An investigation of drop size distribution of rainfall in Thailand. PhD dissertation, Asian Institute of Technology, Bangkok,

Best AC. 1950. The size distribution of raindrops. *Quarterly Journal of the Royal Meterological Society* **76**: 16–36.

Bradford JM. 1986. Penetrability. In Methods of Soil Analysis, Part 1, Klute A (ed.). Physical and Mineralogical Methods–Agronomy Monograph No. 9 (second edition). American Society of Agronomy–Soil Science Society of America: Madison, WI; 463–478.

Bryan RB. 1996. Erosional response to variations in interstorm weathering conditions. In Advances in Hillslope Processes, Vol. 1, Anderson, MG Brooks SM (eds). John Wiley and Sons: Chichester; 589–612.

Bryan RB, Poesen J. 1989. Laboratory experiments on the influence of slope length on runoff, percolation and rill development. *Earth Surface Processes and Landforms* **14**: 211–231.

Coker RJ, Fahey BD, Payne JJ. 1993. Fine sediment production from truck traffic, Queen Charlotte Forest, Marlborough Sounds, New Zealand. *Journal of Hydrology (NZ)* **31**: 56–64.

Elliot WJ, Foltz RB, Luce CH. 1995. Validation of the water erosion prediction project (WEPP) model for low-volume forest roads. Conference Proceedings 6, Sixth International Conference on Low-Volume Roads, Minneapolis, MN, 25–29 June 1995. National Academy Press: Washington D.C.; 178–186.

Fox J, Krummel J, Yarnasarn S, Ekasingh M, Podger N. 1995. Landuse and landscale dynamics in northern Thailand: Assessing change in three upland watersheds since 1954. *Ambio* **24**(6): 328–334.

Gagnon J, Roth JM, Finzer WF, Haycock KA, Feldman DS Jr, Simpson J. 1989. Super *ANOVA*^{TM} *– Accessible General Linear Modeling*. Abacus Concepts, Inc.: Berkeley, CA.

Hess A, Koch KE (compilers). 1979. Geological Map of Thailand, Scale 1:250 000. Federal Institute for Geosciences and Natural Resources: Stuttgart, Germany.

Kubiniok J. 1992. Soils and weathering as indicators of landform development in the mountains and basins of Northern Thailand. *Zeitschrift für Geomorphologie NF*. **91**: 67–78.

Merz W, Bryan RB. 1993. Critical conditions for rill initiation on sandy loam Brunisols: Laboratory and field experiments in southern Ontario, Canada. *Geoderma* **57**: 357–385.

Mualem Y, Assouline S. 1986. Mathematical model for rain drop distribution and rainfall kinetic energy. *Transactions of the ASAE* **29**(2): 494–500.

Reid LM, Dunne T. 1984. Sediment production from forest road surfaces. *Water Resources Research* **20**: 1753–1761.

Schmidt-Vogt D. 1998. Defining degradation: The impacts of swidden on forests in northern Thailand. *Mountain Research and Development* **18**(2): 135–149.

Smith RE, Goodrich DC, Quinton JN. 1995. Dynamic, distributed simulation of watershed erosion: the KINEROS2 and EUROSEM models. *Journal of Soil and Water Conservation* **50**(5): 517–520.

Sutherland RA, Wan Y, Ziegler AD, Lee C-T, El Swaify SA. 1996. Splash and wash dynamics: An experimental investigation using an Oxisol. *Geoderma* **69**: 85–103.

Ziegler AD, Giambelluca TW. 1997a. Importance of rural roads as source areas for runoff in mountainous areas of northern Thailand. *Journal of Hydrology* **196**(1/4): 204–229.

Ziegler AD, Giambelluca TW. 1997b. Simulation of runoff and erosion on mountainous roads in northern Thailand: a first look. In: Human Impact on Erosion and Sedimentation (Proceedings of Rabat Symposium S6, April 1997). IAHS Publication No. 245: 21–29.

